Available online at www.sciencedirect.com
ScienceDirect
Nuclear Instruments and Methods in Physics Research B 256 (2007) 172–176
NIM B
Beam Interactions with Materials & Atoms
www.elsevier.com/locate/nimb

Calculation of the energy loss of swift H and He ions in Ag using the dielectric formalism: The role of inner-shell ionization

Isabel Abril [a], Juan Carlos Moreno-Marín [b], José M. Fernández-Varea [c], Cristian D. Denton [a], Santiago Heredia-Avalos [d,*], Rafael Garcia-Molina [d]

[a] Departament de Física Aplicada, Universitat d'Alacant, Apartat 99, E-03080 Alacant, Spain
[b] Departament de Física, Enginyeria de Sistemes i Teoria del Senyal, Universitat d'Alacant, Apartat 99, E-03080 Alacant, Spain
[c] Facultat de Física (ECM), Universitat de Barcelona, Diagonal 647, E-08028 Barcelona, Spain
[d] Departamento de Física – ClOyN, Universidad de Murcia, Apartado 4021, E-30080 Murcia, Spain

Available online 16 January 2007

Abstract

The electronic energy loss of swift H and He ions in solid Ag is studied theoretically within the dielectric formalism, considering the different equilibrium charge states of the projectile inside the target. Excitation of the weakly-bound (outer) electrons is described by a superposition of Mermin-type energy-loss functions, whereas the contribution to the projectile energy loss due to the ionization of the K, L and M shells of the Ag atoms is included through hydrogenic or numerical generalized oscillator strengths. This method is used to evaluate the stopping power and the energy-loss straggling parameter of H and He ions in Ag as a function of the projectile energy, showing a good agreement with available experimental data. The contribution of the target inner-shells to the energy loss begins to be appreciable at projectile energies larger than a few hundred keV/u, being more important for the energy-loss straggling parameter than for the stopping cross section.

PACS: 34.50.Bw; 77.22.−d

Keywords: Energy loss; Stopping power; Energy straggling; Dielectric function

Quantitative knowledge of the energy loss of fast charged particles in matter finds many practical applications in different areas such as microelectronics, surface analysis, nuclear physics, space exploration, radiation protection or cancer therapy [1–4]. Although a lot of experimental work has been done on this subject, with different projectiles and targets, the theoretical treatment is necessary because it allows a more profound understanding of the mechanisms that cause the energy loss. Furthermore, theory enables to fill the gaps where there is a lack of experimental data for certain combinations of projectile, target and energy range. The dielectric formalism has been widely used to study the energy loss of swift light ions in solids [5]. However, materials such as Ag and other transition metals have a dielectric function that cannot be regarded as that of a simple free-electron gas and thus require a more elaborate description.

In the present work, we evaluate the stopping power and the energy-loss straggling parameter of metallic Ag for swift H and He ions using the dielectric formalism with a realistic representation of the target electromagnetic excitations spectrum. We take into account screening effects, the polarization of the ion, and the energy loss due to electron capture and loss processes; the different equilibrium charge states that the projectile can have during its motion through the target are included by means of their charge-state fractions at equilibrium. The projectile electron density is described by the statistical model devised by Brandt

* Corresponding author. Fax: +34 968 36 41 48.
E-mail address: sheredia@um.es (S. Heredia-Avalos).

0168-583X/$ - see front matter © 2006 Elsevier B.V. All rights reserved.
doi:10.1016/j.nimb.2006.11.109

and Kitagawa (BK hereafter) [6,7] or by hydrogenic orbitals, whereas the energy-loss function (ELF) of Ag is characterized by a linear combination of Mermin-type ELFs to account for outer-electron excitations and generalized oscillator strengths (GOS) to include the ionization of the K, L and M inner-shell electrons. Two models of the GOS are considered, namely the hydrogenic approach [8–11] and a more sophisticated numerical calculation [12]. In this study, we focus our attention on the influence of these descriptions of the GOS on the stopping power and the energy-loss straggling parameter.

When a heavy charged particle with atomic number Z_1, mass M_1 and velocity v (kinetic energy $E = M_1 v^2/2$) penetrates a material it loses kinetic energy through inelastic interactions. In the energy range we are concerned, $10\ \mathrm{keV/u} \lesssim E/M_1 \lesssim 10\ \mathrm{MeV/u}$, the energy loss is mainly due to the excitation and ionization of target electrons by the passing ion (nuclear stopping power is negligible). The projectile can also capture electrons from or lose electrons to the stopping material, thus changing its charge state q ($0 \leqslant q \leqslant Z_1$). When charge equilibrium is reached, the probability ϕ_q of finding the ion in a given charge state q is stationary and depends only on v. Using this charge-state approach we can express the stopping power S, i.e. the mean energy lost by the projectile per unit path length, as

$$S(v) = \sum_{q=0}^{Z_1} \phi_q(v) S_q(v) + S_{\mathrm{CL}}(v), \tag{1}$$

where S_q is the stopping power corresponding to the charge state q. The charge-state fractions at equilibrium, ϕ_q, are evaluated from the CasP 3.1 code [13]. Within the dielectric formalism, the stopping power S_q of a material for an ion with charge state q is given by

$$S_q(v) = \frac{2e^2}{\pi v^2} \int_0^\infty \frac{\mathrm{d}k}{k} \rho_q^2(k) \int_0^{kv} \mathrm{d}\omega\ \omega\ \mathrm{Im}\left[\frac{-1}{\epsilon(k,\omega)}\right], \tag{2}$$

where e is the absolute value of the electron charge, $\rho_q(k)$ is the Fourier transform of the projectile charge density for the charge state q, $\hbar k$ and $\hbar\omega$ are, respectively, the momentum and energy transferred to electronic excitations of the target, and $\mathrm{Im}[-1/\epsilon(k,\omega)]$ is the ELF of the stopping material. The contribution S_{CL} due to electron capture and loss events is obtained by an extension of the model proposed in [14].

The fluctuations of the energy loss around the average value, dictated by the stopping power, are quantified by the energy-loss straggling parameter Ω^2, defined as the variance in the energy-loss distribution per unit path length. In the same way as S, Ω^2 can be written as a sum over the possible charge states,

$$\Omega^2(v) = \sum_{q=0}^{Z_1} \phi_q(v) \Omega_q^2(v), \tag{3}$$

where the partial contributions Ω_q^2 can be expressed in the dielectric formalism as

$$\Omega_q^2(v) = \frac{2e^2\hbar}{\pi v^2} \int_0^\infty \frac{\mathrm{d}k}{k} \rho_q^2(k) \int_0^{kv} \mathrm{d}\omega\ \omega^2\ \mathrm{Im}\left[\frac{-1}{\epsilon(k,\omega)}\right]. \tag{4}$$

The Fourier transforms of the charge density $\rho_q(k)$ for the light ions H and He will be represented in two manners. One is the widely-used BK method [6,7] in which all the electrons bound to the ion are characterized by a generic orbital. Another way to model $\rho_q(k)$ consists of using hydrogenic wave functions. For projectile charge states with two electrons, i.e. in the case of neutral He, it is necessary to consider the screening of the interaction between the nucleus of the projectile and its electrons; this screening is described replacing Z_1 by an effective nuclear charge $Z_{1,\mathrm{eff}}$ given by Slater's rules [15]. The dynamic screening of the interaction by the target electrons originates a further reduction of the effective nuclear charge. This additional screening is included resorting to a Yukawa potential replacing $Z_{1,\mathrm{eff}}$ by $Z_{1,\mathrm{eff}} \exp(-\langle r\rangle/a)$, where a is the screening length, which depends on the target electronic density and on the projectile velocity [16], and $\langle r\rangle$ is the average value of the electron-nucleus distance (for instance, $\langle r\rangle = 3/2$ a.u. for hydrogen atoms) [9,14]. Furthermore, our calculations also account for the polarization of the projectile caused by the electric field it induces in the target. This self-induced electric field displaces the center of the ion's electronic cloud from its nucleus, and then the stopping power must be calculated for the projectile nucleus, its electronic cloud, and a term due to interference effects [11,14].

The ELF contains all the information about the excitations that the target can sustain, and therefore allows the knowledge of the stopping properties of a given material. A method that has proven its reliability is the one designed by Abril et al. [17]. In this approach the contributions to the ELF of the outer electron excitations and of the inner-shell ionizations are explicitly separated,

$$\mathrm{Im}\left[\frac{-1}{\epsilon(k,\omega)}\right] = \mathrm{Im}\left[\frac{-1}{\epsilon(k,\omega)}\right]_{\mathrm{outer}} + \mathrm{Im}\left[\frac{-1}{\epsilon(k,\omega)}\right]_{\mathrm{inner}}. \tag{5}$$

The description of the weakly-bound outer shells is performed by fitting the experimental optical ELF, $\mathrm{Im}[-1/\epsilon(k=0,\omega)]_{\mathrm{exp}}$, to a sum of Mermin-type ELFs

$$\mathrm{Im}\left[\frac{-1}{\epsilon(k=0,\omega)}\right]_{\mathrm{outer}} = \sum_i A_i \mathrm{Im}\left[\frac{-1}{\epsilon_{\mathrm{M}}(\omega_i,\gamma_i;k=0,\omega)}\right], \tag{6}$$

where ϵ_{M} is the Mermin dielectric function [18]. In the above expression ω_i and γ_i are related to the position and width, respectively, of the ith Mermin-type ELF, while the coefficients A_i are the corresponding weights. The advantage of this method is that the fit of the ELF in the optical limit ($k = 0$) is analytically extended to $k \neq 0$ through the properties of the Mermin dielectric function [19]. In turn, inner-shell electrons have large binding energies, displaying a marked atomic character and no collective effects; they can thus be suitably modelled by means

of atomic GOSs [20]. Then $\mathrm{Im}[-1/\epsilon(k,\omega)]_{\mathrm{inner}}$ in atomic units, in atomic units, is obtained from the relation [20]

$$\mathrm{Im}\left[\frac{-1}{\epsilon(k,\omega)}\right]_{\mathrm{inner}} = \frac{2\pi^2\mathscr{N}}{\omega}\sum_{n\ell}\frac{\mathrm{d}f_{n\ell}(k,\omega)}{\mathrm{d}\omega}, \tag{7}$$

where $\mathscr{N}$ is the density of atoms in the target and $\mathrm{d}f_{n\ell}(k,\omega)/\mathrm{d}\omega$ is the GOS of the (n,ℓ) subshell.

We consider two methods to evaluate the GOS. The first one assigns hydrogenic wave functions to the inner-shells of the target atoms, with effective nuclear charges for each shell given by Slater's rules [9]. The advantage of this procedure is that analytical expressions exist for the non-relativistic hydrogenic GOSs (see e.g. the appendix of [9]). A more precise treatment is the *ab initio* numerical evaluation of the required GOSs [12]. Within the plane-wave Born approximation, the initial and final wave functions of the projectile are taken as plane waves, whereas the active electron moves in the potential of the target atom. We have adopted a Dirac–Hartree–Fock–Slater self-consistent potential for the present calculations, because correlation effects are relatively unimportant for atomic inner-shells. In this context it is customary to describe the inelastic collision by means of $W \equiv \hbar\omega$ (energy transfer) and $Q \equiv \hbar^2k^2/2m_e$ ("recoil" energy), in terms of which the non-relativistic GOS is expressed as

$$\frac{\mathrm{d}f_{n\ell}(Q,W)}{\mathrm{d}W} = \frac{W}{Q}\sum_{\ell'}(2\ell'+1)\sum_{\lambda}(2\lambda+1)\begin{pmatrix}\ell' & \lambda & \ell\\ 0 & 0 & 0\end{pmatrix}^2 R^{(\lambda)}_{n\ell,\mathscr{E}\ell'}(k)^2, \tag{8}$$

where (:::) are Wigner's $3j$ symbols and the radial integrals are

$$R^{(\lambda)}_{n\ell,\mathscr{E}\ell'}(k) \equiv \int_0^\infty P_{\mathscr{E}\ell'}(r)\, j_\lambda(kr)\, P_{n\ell}(r)\,\mathrm{d}r. \tag{9}$$

Here j_λ are spherical Bessel functions. The initial (bound) and final (free) reduced radial wave functions $P_{n\ell}(r)$ and $P_{\mathscr{E}\ell'}(r)$ of the active electron are obtained by solving numerically the Schrödinger equation, for the selected atomic potential, with the aid of the RADIAL subroutine package [21]; $\mathscr{E}$ is the kinetic energy of the ejected electron in the final state $(\mathscr{E},\ell')$ and $W = \mathscr{E} + U_{n\ell}$, where $U_{n\ell}$ is the binding energy of the (n,ℓ) subshell. Enough ℓ' terms are included in the sums of Eq. (8) so as to ensure convergence to better than 0.1%.

In Fig. 1 we depict the ELF of Ag in the optical limit ($k = 0$). The symbols and the dashed curve are experimental results [22,23], whereas the solid curve is our fit according to the outlined method, including the contribution of the outer and the inner electrons. The excitation spectrum pertaining to the outer electrons was fitted by a sum of 4 Mermin-type ELFs; the obtained parameters are listed in Table 1. The contribution to the ELF from ionization of the K, L and M shells was calculated with hydrogenic

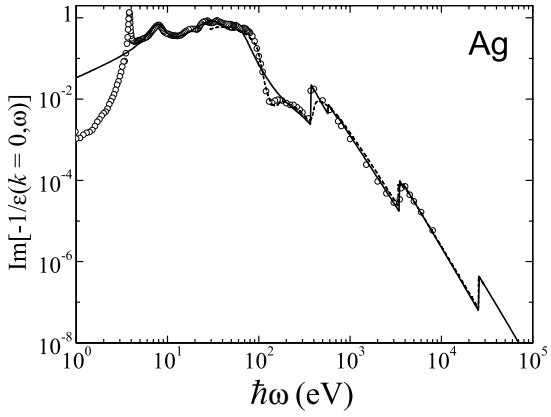

Fig. 1. ELF of Ag in the optical limit ($k = 0$) as a function of the excitation energy $\hbar\omega$. The solid curve corresponds to our model, while the symbols and the dashed curve represent the experimental data [22] and the experimental results from X-ray scattering factors [23], respectively.

Table 1
Parameters used to fit, through Eq. (6), the low-energy region of the ELF of Ag

Material	i	$\hbar\omega_i$ (eV)	$\hbar\gamma_i$ (eV)	A_i
Ag ($D = 10.5$ g/cm^3)	1	7.891	35.37	2.378×10^{-1}
	2	33.20	29.93	6.618×10^{-1}
	3	62.58	29.93	1.745×10^{-1}
	4	285.7	353.7	2.779×10^{-3}

D is the mass density of the target.

GOSs; the onset of each subshell is visible as a sharp rise in the ELF at the corresponding threshold energies. Besides reproducing the main trends of the experimental ELF we demanded that the fitted ELF satisfies the f-sum rule. As an additional check, we have evaluated the mean excitation energy and obtained $I = 440$ eV, which compares satisfactorily with the currently accepted value 470 ± 10 eV [24].

The stopping cross section (SCS) is often used to quantify the average energy loss per unit path length instead of the stopping power, because it removes the dependence on the density of atoms $\mathscr{N}$; it is defined as $\mathrm{SCS} = S/\mathscr{N}$.

The SCSs of Ag for H and He ions are displayed in Fig. 2. The solid and dashed curves are our theoretical SCSs when the BK model or hydrogenic wave functions, respectively, are employed to describe the electronic density of the projectile. The symbols correspond to experimental data, extracted from Paul's webpage [25]. The agreement with the experimental results is quite good in a wide range of energies. We recall that our calculations include the energy loss arising from electron capture and loss events; for H ions S_{CL} is ~3% of the total SCS at 100 keV/u and ~13% at 10 keV/u, whereas for He S_{CL} becomes less important, being ~2% of the total SCS at 100 keV/u and ~5% at 10 keV/u. The dot-dashed curves in Fig. 2 represent the SCSs due to only inner-shell ionization, evaluated with the analytical hydrogenic GOSs; similar results (within 15%) were obtained with the numerical GOSs. The contribution of the inner-shells to the SCSs is very

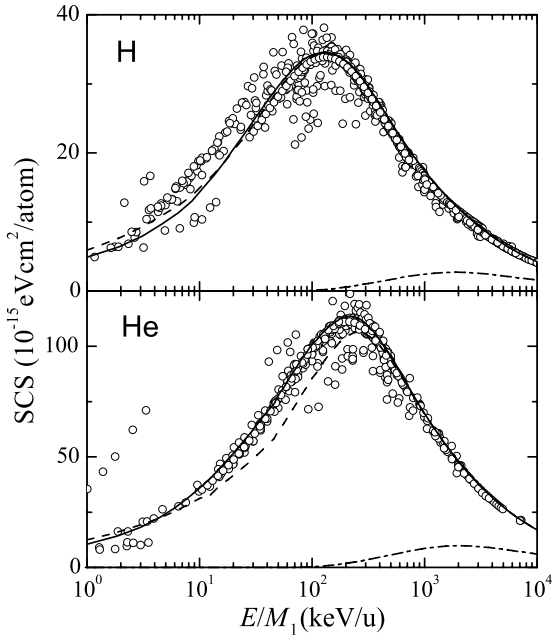

Fig. 2. SCSs of Ag for H and He ions as a function of energy per atomic mass unit. The solid and dashed curves are the SCSs calculated with the BK model and hydrogenic wave functions to describe $\rho_q(k)$, respectively. The symbols indicate experimental data, taken from [25]. The dot-dashed curves correspond to the SCSs due to inner-shell ionization evaluated with hydrogenic GOSs.

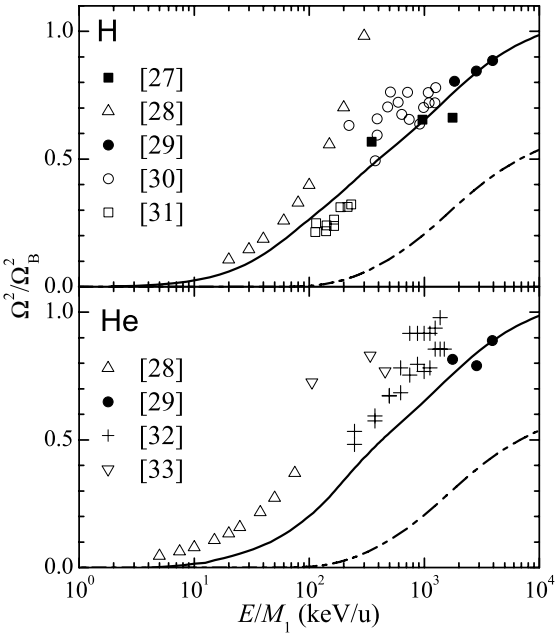

Fig. 3. Reduced energy-loss straggling parameters of Ag for H and He ions as a function of energy per atomic mass unit. The solid curves are the straggling parameters calculated with the BK model of $\rho_q(k)$. The symbols indicate experimental values [27–33]. The dot-dashed curves correspond to the reduced straggling parameters due to inner-shell ionization, evaluated with hydrogenic GOSs.

small below ~100 keV/u. At 1 MeV/u, it amounts to ~15% of the total SCS for the two ions, increasing with energy until a maximum is reached and decreasing afterwards. The inner-shell contribution to the SCS does not depend on the model adopted for $\rho_q(k)$, because at these high energies the projectile travels as a bare charged particle.

The two considered models of $\rho_q(k)$ yield similar SCSs for H ions; on the other hand, for He we find significant differences between them up to ~400 keV/u, where the He ion becomes fully stripped. Although the hydrogenic model describes the projectile in a more realistic way than the BK model, the latter is in better agreement with the experimental SCSs. In order to determine the origin of this contradictory result a more accurate calculation of S_{CL} should be made first [26] (replacing our simple estimate [14]), an issue worthy of a careful analysis that exceeds the purpose of the present paper. All the same, our main goal in this work is to study the role of inner-shell ionization in the energy loss of fast ions, which only becomes sizeable at high energies, i.e. where the projectile is almost fully stripped of its electrons and, therefore, no differences appear in the results provided by these models for the SCSs. Moreover, the ionization of the target inner-shells involves close collisions with the projectile and in this case the description of the ion's electron cloud becomes unimportant.

Fig. 3 shows the reduced energy-loss straggling parameters Ω^2/Ω_B^2 of Ag for H and He ions; $\Omega_B^2 = 4\pi e^4 \mathcal{N} Z_1^2 Z_2$ is Bohr's straggling parameter and Z_2 is the atomic number of the target. The solid curves are our theoretical calculations with the BK model of $\rho_q(k)$; almost identical results were obtained when hydrogenic wave functions were used instead. The symbols represent available experimental data from the literature [27–33]. The theoretical results compare satisfactorily with the measurements in a wide range of energies, especially in the case of H. It should be kept in mind that some of the older measurements may overestimate Ω^2 because inhomogeneities in the samples lead to larger experimental values of the straggling parameter. The dot-dashed curves in Fig. 3 represent the reduced energy-loss straggling parameter due to inner-shells, calculated with the hydrogenic GOSs; the differences between the hydrogenic and numerical GOSs are again small. The contribution of the inner-shells to Ω^2/Ω_B^2 becomes visible above ~100 keV/u for both H and He projectiles, and it increases steadily with energy, reaching ~60% of the total energy-loss straggling parameter at $E/M_1 \gtrsim 10$ MeV/u; notice that the number of electrons in the K, L and M shells of Ag ($Z_2 = 47$) is 28, and $28/47 \approx 0.596$. Therefore, at high energies the role of the inner shells is more important for Ω^2 than for the SCS. This behaviour can be understood in the light of the dependencies on ω of Eqs. (2) and (4).

The SCSs and reduced straggling parameters pertaining to the ionization of each inner subshell by H^+ ions are displayed in Fig. 4 as a function of the projectile energy. The solid and dashed curves were obtained with the hydrogenic and numerical GOSs, respectively. In most cases the agreement between the two GOS models is rather good, being both curves indistinguishable. The largest differences occur

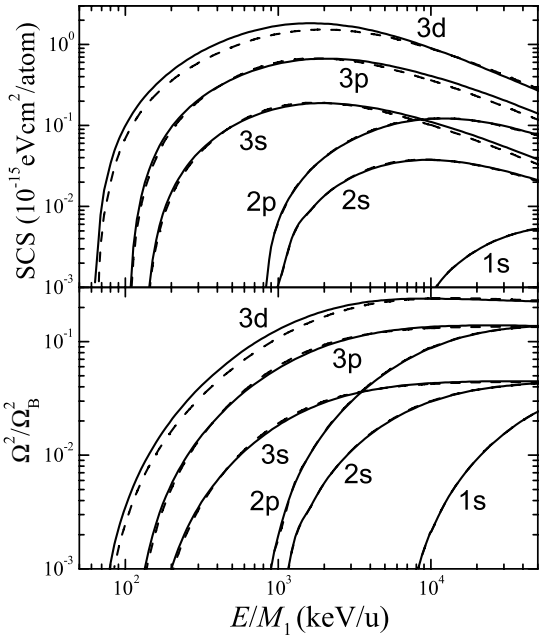

Fig. 4. Contributions of the indicated subshells of Ag to the SCS and reduced straggling parameter of H^+ ions as a function of energy per atomic mass unit; the corresponding contributions for He^{2+} ions are 4 times larger. The solid and dashed curves have been calculated with hydrogenic and numerical GOSs, respectively.

for the 3d subshell. Although this subshell contributes to the stopping magnitudes more than the other subshells, its contribution is only significant at energies much larger than the corresponding threshold energy, where the hydrogenic GOS closely reproduces the numerical GOS. The relative importance of the deeper inner-shells is much smaller, so that even substantial discrepancies between the hydrogenic and numerical GOSs will have a limited impact on the total SCS and Ω^2. For instance, relativistic effects modify the GOSs of deep inner-shells, but the stopping magnitudes are very insensitive to their contribution.

In summary, we have calculated the stopping cross section and energy-loss straggling parameter of Ag for swift H and He ions, obtaining a fairly good agreement with the available experimental data in a broad energy range. The contribution of the K, L and M shells to the SCS and Ω^2 has been evaluated with either hydrogenic or numerical GOSs. It turns out that the analytical hydrogenic GOSs describe reasonably well the contribution of inner-shell ionizations to these stopping magnitudes. As a consequence, the use of more accurate, but also cumbersome, *ab initio* numerical calculations of the GOSs seems to be unnecessary in this context.

Acknowledgements

This work has been financially supported by the Spanish Ministerio de Educación y Ciencia (projects BFM2003-04457-C02-01 and BFM2003-04457-C02-02). S.H.A. thanks the Fundación CajaMurcia for financial assistance and C.D.D. thanks the Spanish Ministerio de Educación y Ciencia for support under the Ramón y Cajal Program.

References

[1] S.A. Campbell, The Science and Engineering of Microelectronic Fabrication, Oxford University Press, Oxford, 1996.
[2] M.A. Kumakhov, F.F. Komarov, Energy Loss and Ion Ranges in Solids, Gordon and Breach, New York, 1981.
[3] J. Turner, Atoms, Radiation and Radiation Protection, second ed., Wiley, New York, 1995.
[4] G. Kraft, Nucl. Instr. and Meth. A 454 (2000) 1.
[5] J. Lindhard, K. Dan, Vidensk. Selsk. Mat.-Fys. Medd. 28 (8) (1954).
[6] W. Brandt, M. Kitagawa, Phys. Rev. B 25 (1982) 5631.
[7] W. Brandt, Nucl. Instr. and Meth. 194 (1982) 13.
[8] J.C. Moreno-Marín, I. Abril, R. Garcia-Molina, Nucl. Instr. and Meth. B 193 (2002) 30.
[9] S. Heredia-Avalos, R. Garcia-Molina, J.M. Fernández-Varea, I. Abril, Phys. Rev. A 72 (2005) 052902.
[10] R. Garcia-Molina, I. Abril, C.D. Denton, S. Heredia-Avalos, Nucl. Instr. and Meth. B 249 (2006) 6.
[11] J.C. Moreno-Marín, I. Abril, S. Heredia-Avalos, R. Garcia-Molina, Nucl. Instr. and Meth. B 249 (2006) 29.
[12] S. Segui, M. Dingfelder, J.M. Fernández-Varea, F. Salvat, J. Phys. B: Atom. Mol. Opt. Phys. 35 (2002) 33.
[13] P.L. Grande, G. Schiwietz, CasP, Convolution approximation for swift Particles, version 3.1, 2005. <http://www.hmi.de/people/schiwietz/casp.html>.
[14] S. Heredia-Avalos, R. Garcia-Molina, Nucl. Instr. and Meth. B 193 (2002) 15.
[15] J.C. Slater, Phys. Rev. 36 (1930) 57.
[16] S. Heredia-Avalos, R. Garcia-Molina, N.R. Arista, Europhys. Lett. 54 (2001) 729.
[17] I. Abril, R. Garcia-Molina, C.D. Denton, F.J. Pérez-Pérez, N.R. Arista, Phys. Rev. A 58 (1998) 357.
[18] N.D. Mermin, Phys. Rev. B 1 (1970) 2362.
[19] D.J. Planes, R. Garcia-Molina, I. Abril, N.R. Arista, J. Electron Spectrosc. Relat. Phenom. 82 (1996) 23.
[20] R.F. Egerton, Electron Energy-Loss Spectroscopy in the Electron Microscope, Plenum Press, New York, 1989.
[21] F. Salvat, J.M. Fernández-Varea, W. Williamson Jr., Comput. Phys. Commun. 90 (1995) 151.
[22] E.D. Palik, G. Ghosh (Eds.), The Electronic Handbook of Optical Constants of Solids, Academic Press, San Diego, 1999.
[23] B.L. Henke, E.M. Gullikson, J.C. Davis, Atom. Data Nucl. Data Tables 54 (1993) 181, The ASCII files for the f_1 and f_2 scattering factors of the different elements can be downloaded from <http://xray.uu.se/hypertext/henke.html>.
[24] ICRU Report 49, Stopping powers and ranges for protons and alpha particles, in: International Commission on Radiation Units and Measurements, Bethesda, 1993.
[25] H. Paul, Experimental Stopping Power Compilation. <http://www.exphys.uni-linz.ac.at/Stopping/>.
[26] A. Arnau, M. Peñalba, P.M. Echenique, F. Flores, R.H. Ritchie, Phys. Rev. Lett. 65 (1990) 1024.
[27] W. Möller, U. Nocken, Nucl. Instr. and Meth. 149 (1978) 177.
[28] J.C. Eckardt, Phys. Rev. A 18 (1978) 426.
[29] F. Besenbacher, J.U. Andersen, E. Bonderup, Nucl. Instr. and Meth. 168 (1980) 1.
[30] J. Lombaard, J. Conradie, E. Friedland, Nucl. Instr. and Meth. 216 (1983) 293.
[31] Y. Kido, T. Koshikawa, Phys. Rev. A 44 (1991) 1759.
[32] J.Y. Hsu, J.H. Liang, Y.C. Yu, K.M. Chen, Nucl. Instr. and Meth. B 241 (2005) 160.
[33] G.E. Hoffman, D. Powers, Phys. Rev. A 13 (1976) 2042.